Free-boundary models of a meltwater conduit

Dallaston, MC & Hewitt, IJ

Free-boundary models of a meltwater conduit

Michael. C. Dallaston[a)] and Ian. J. Hewitt

Mathematical Institute, University of Oxford

We analyse the cross-sectional evolution of an englacial meltwater conduit that contracts due to inward creep of the surrounding ice and expands due to melting. Making use of theoretical methods from free-boundary problems in Stokes flow and Hele–Shaw squeeze flow we construct an exact solution to the coupled problem of external viscous creep and internal heating, in which we adopt a Newtonian approximation for ice flow and an idealized uniform heat source in the conduit. This problem provides an interesting variant on standard free-boundary problems, coupling different internal and external problems through the kinematic condition at the interface. The boundary in the exact solution takes the form of an ellipse that may contract or expand (depending on the magnitudes of effective pressure and heating rate) around fixed focal points. Linear stability analysis reveals that without the melting this solution is unstable to perturbations in the shape. Melting can stabilize the interface unless the aspect ratio is too small; in that case, instabilities grow largest at the thin ends of the ellipse. The predictions are corroborated with numerical solutions using boundary integral techniques. Finally, a number of extensions to the idealized model are considered, showing that a contracting circular conduit is unstable to all modes of perturbation if melting occurs at a uniform rate around the boundary, or if the ice is modelled as a shear-thinning fluid.

[a)]Electronic mail: Michael.Dallaston@maths.ox.ac.uk

I. INTRODUCTION

Melt or rainwater that runs into the body of an ice sheet flows through a network of conduits, both englacially and subglacially (*i.e.* within the ice, and between the ice and the underlying bedrock)[1]. The size and shape of these conduits is governed by two competing effects: melting, due to viscous dissipation and heat advected by the water flow, and inward creep due to the surrounding ice flow. The latter occurs because the water pressure is less than the cryostatic pressure in the ice; on time scales greater than around a day, glacier ice behaves as a viscous, shear thinning fluid[2].

A model for these competing effects was developed by Röthlisberger[3], and similar models are becoming an important component of modern ice-sheet simulations[4]. A chief assumption in Röthlisberger's model is that conduits are circular in cross-section (or semicircular if at the base of the glacier, which is then made equivalent to a circle by symmetry). Under that assumption, an exact solution for a contracting circular cavity in a power-law fluid may be used to describe the ice creep[5]. Combined with a parameterization for the wall melting, this provides a simple evolution equation for the conduit's cross-sectional area that can be included in glacier-scale drainage models. For instance, some models feature networks of such conduits[6], or interaction with a distributed drainage system[7].

In practice, conduits are rarely observed to be circular in cross section. In fact, as we discuss in this paper, there are theoretical reasons why one might expect them not to be circular, since the simple contraction of a circular cavity is in fact unstable to perturbations in its shape. There are relatively few theoretical studies that have not assumed circular symmetry, however. Hooke[8] prescribed the shape as a circular segment instead, and Ng[9] considered a slender channel approximation. Numerical modelling using finite elements has been undertaken by Cutler[10], and a related problem of open-channel flow on the glacier surface was considered by Jarosch & Gudmundsson[11].

Our aim in this paper is to examine the evolution of a conduit cross-section without making any *a priori* assumptions about its shape. To this end, we use idealized models that enable us to draw on the connection with other two-dimensional free-boundary viscous flow problems. The literature on such problems is extensive[12]. Although the free boundary makes them generally nonlinear and highly nontrivial (at least when symmetry is not assumed), the application of complex variable theory has enabled the construction of many families of

explicit solutions, usually in the form of conformal mapping functions that transform a fixed domain to the evolving fluid domain. We adopt some of these methods to develop exact solutions for the conduit shape and to analyse its stability.

In section II we formulate a model of the meltwater conduit and outline related mathematical concepts. The model incorporates the inward creep of a viscous fluid surrounding a two-dimensional cavity, and melting at the cavity interface caused by heat generation within it. We take the creeping flow to be Newtonian, and the heat to be generated uniformly throughout the cavity, with the temperature governed by Poisson's equation and a Stefan condition at the interface. While this may not be an accurate description of dissipation in turbulent water flow, it allows significant analytic progress to be made while accounting for the effect of both creep and melting. The external and internal problems are coupled together through the kinematic condition at the interface. Independently, these external and internal problems correspond to previously studied problems in the free boundary literature; the external creep of ice is equivalent to a contracting bubble in Stokes flow[13–15], and the melting due to uniform heating is equivalent to the problem of Hele–Shaw *squeeze* flow[15–18], where a viscous fluid is pressed between two plates. The interesting and novel aspect of this paper is the combination of both creep due to the external Stokes problem *and* melting due to the internal heating problem.

In section III we examine some of the exact solutions for each of the two free-boundary problems. Considered independently, both the Stokes and heating problems have a solution in which the free boundary is an ellipse that contracts or grows while remaining confocal (that is, with fixed focal points). Consequently, such ellipses are also solutions of the coupled problem. Of course, a circle is a special case of this solution. A steady-state may occur if the effective pressure and heating are in balance; for a given pressure, a thinner ellipse requires a greater amount of heating to be steady. Ellipses have arisen previously as exact solutions to two-phase harmonic[19,20] and biharmonic[21] free boundary problems, although to our knowledge this is the first example which features both harmonic (heating) and biharmonic (Stokes flow) fields in a single problem. From the exact solutions we also surmise that the aspect ratio of a contracting cavity increases, and that cavities that have a small aspect ratio will contract faster than the circular cavity-based model suggests; in fact, a non-circular elliptical cavity can close in finite time, whereas a circular one can only decrease in area exponentially. A similar result has also been found in less idealized numerical models[10].

In section IV we consider the stability of the circle or ellipse to perturbations. The mathematical theory predicts that contracting free boundaries in Stokes flow alone are unstable, and form cusps in finite time[13,14]. This instability has been observed in (non-ice related) experiments, although in the context of a compressed planar surface rather than a contracting circle[22]. The addition of melting at the boundary might be expected to introduce diffusive effects that ameliorate this instability; indeed we find that our model of uniform heating in the conduit stabilizes the interface to a certain extent. We show that the stability depends only on the aspect ratio; a sufficiently fat ellipse (large aspect ratio) is stable to perturbations, but becomes unstable to higher frequency modes as it becomes thinner (that is, as aspect ratio tends to zero). The instability is largest near the ends of the ellipse, where curvature is greatest. We demonstrate the results using numerical boundary integral methods that are adapted from those previously applied to free-boundary Stokes flow[23–25]. The numerical solutions suggest that cusps may form when the aspect ratio is smaller than the critical value found from the linear stability analysis.

We conclude in section V with a discussions of extensions to the model. Firstly we consider the possibility of feedback between the cross-sectional area and the heating rate, as is included in the Röthlisberger channel theory. We also discuss linear stability and numerical results when the heating is assumed to be confined to the interface so that the melt rate is uniform along the perimeter. In that case the circle remains unstable to all perturbations, but with nonzero melting, the instability intriguingly results in inward-pointing corners, rather than outward-pointing cusps. Lastly we include a stability analysis for the case of a contracting circle surrounded by a shear-thinning power law fluid, as may be more appropriate for ice. As in the Newtonian case, the interface is unstable to all modes of perturbation; the major difference is that lower frequency modes of perturbation are less unstable than higher frequency ones.

II.   MATHEMATICAL FORMULATION

The mathematical model consists of two distinct systems, each posed in a region of the plane: a model for the viscous flow of ice in a region $\Omega_i(t)$ outside a simple closed curve $\partial\Omega(t)$, and a model of heat flow in the region $\Omega_c(t)$ inside $\partial\Omega(t)$ (see figure 1). The curve $\partial\Omega(t)$ represents the conduit wall, and the kinematic condition at this interface couples the
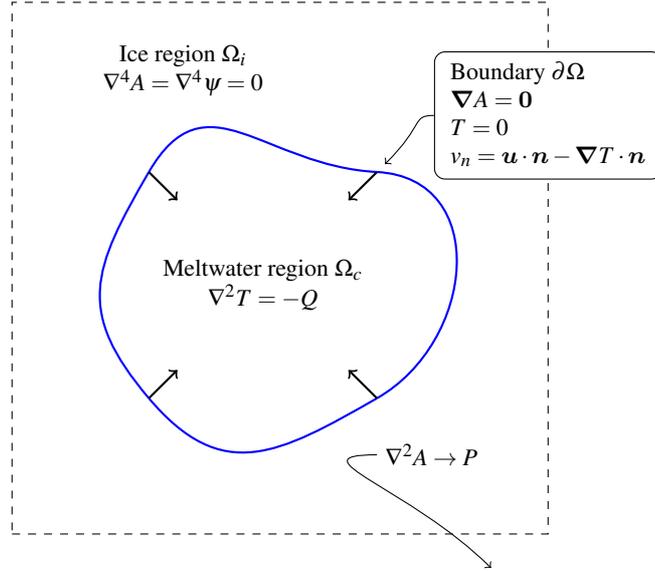
4

FIG. 1. A schematic of the coupled creep closure/melting free boundary problem (1), (9), (10).

external and internal problems.

A. Stokes flow

The flow of ice in Ω_i is modelled using Newtonian Stokes flow, with the stress tensor $\boldsymbol{\sigma}$ and velocity vector $\boldsymbol{u}$ satisfying

$$\boldsymbol{\nabla} \cdot \boldsymbol{\sigma} = \boldsymbol{0}, \qquad \boldsymbol{\nabla} \cdot \boldsymbol{u} = 0, \qquad \boldsymbol{\sigma} = -p\boldsymbol{I} + \mu\boldsymbol{D}, \qquad \qquad \boldsymbol{x} \in \Omega_i. \qquad (1a)$$

Here $\boldsymbol{\sigma}$ has been decomposed into the pressure p and viscous stress tensor $\boldsymbol{\tau}$, which has a linear dependence on the strain rate tensor $\boldsymbol{D} = \boldsymbol{\nabla}\boldsymbol{u} + \boldsymbol{\nabla}^T\boldsymbol{u}$; the coefficient μ is the viscosity. The creep closure is driven by a far field pressure p^∞, and we assume a constant water pressure inside the channel that we take to be zero (thus p^∞ is the pressure difference, referred to in the glaciological context as the *effective* pressure). Neglecting surface tension, the boundary conditions are thus

$$\boldsymbol{\sigma} \cdot \boldsymbol{n} = \boldsymbol{0}, \qquad \qquad \boldsymbol{x} \in \partial\Omega, \qquad (1b)$$

$$p \to p^\infty, \qquad \qquad |\boldsymbol{x}| \to \infty. \qquad (1c)$$

For Newtonian flow it is convenient to formulate the problem in terms of the nondimensional Airy stress function A, whose second partial derivatives give the components of the stress

tensor[14,26]:

$$\boldsymbol{\sigma} = \mu[t] \begin{bmatrix} -A_{yy} & A_{xy} \\ A_{yx} & -A_{xx} \end{bmatrix}. \tag{2}$$

Here $[t]$ is a characteristic time scale, which we leave arbitrary. The Stokes flow problem and boundary conditions (1) are equivalent to

$$\nabla^4 A = 0, \qquad \boldsymbol{x} \in \Omega_i, \tag{3a}$$

$$A = \boldsymbol{\nabla} A \cdot \boldsymbol{n} = 0, \qquad \boldsymbol{x} \in \partial\Omega, \tag{3b}$$

$$\nabla^2 A \to P, \qquad |\boldsymbol{x}| \to \infty, \tag{3c}$$

where $P = p^\infty \mu^{-1}[t]^{-1}$ is the nondimensional far field pressure.

To obtain the velocity components we require the streamfunction ψ, which is related to A by the complex Goursat representation[14]

$$A + \mathrm{i}\psi = \phi(z)\overline{z} + \chi(z), \tag{4}$$

where ϕ and χ, called the Goursat functions, are analytic in Ω_i. In terms of these Goursat functions the complex velocity and the pressure are[14]

$$u + \mathrm{i}v = -\phi + z\overline{\phi'} + \overline{\chi'}, \qquad p = 4\Re(\phi'). \tag{5}$$

B. Heating

Inside the conduit we assume a uniform heat source density q, and solve for the temperature T, with diffusion occurring much faster than the time scale on which the boundary evolves. The temperature thus satisfies Poisson's equation

$$K\nabla^2 T = -q, \qquad \boldsymbol{x} \in \Omega_c, \tag{6}$$

where q is the heat source density and K is the thermal conductivity. On the interface, T is at the constant melting temperature, shifted without loss of generality to zero. We assume the ice is everywhere at the melting temperature, so there is no heat flow in Ω_i; all heat goes into melting at the boundary, leading to a melt rate m given by

$$m = \frac{K}{\rho L} \boldsymbol{\nabla} T \cdot \boldsymbol{n}, \qquad \boldsymbol{x} \in \partial\Omega \tag{7}$$

6

where L is the latent heat. From (7) we find a temperature scale

$$[T] = \frac{\rho L [x]^2}{K[t]},$$ (8)

given a length scale $[x]$, and we see that the neglect of time derivatives from (6) is equivalent to the (reasonable) assumption that the Stefan number, $\rho L / [T]$, is large. The nondimensional temperature now satisfies

$$\nabla^2 T = -Q, \qquad\qquad \boldsymbol{x} \in \Omega_c,$$ (9a)

$$T = 0, \qquad\qquad \boldsymbol{x} \in \partial\Omega,$$ (9b)

where $Q = q[t]\rho^{-1}L^{-1}$ is the nondimensional heat source density.

C.   Coupled interface motion

Under the above scalings the normal velocity of the boundary, v_n, is given by the kinematic condition that includes both the inward creep and melting terms:

$$v_n = \boldsymbol{u} \cdot \boldsymbol{n} - \boldsymbol{\nabla} T \cdot \boldsymbol{n}, \qquad \boldsymbol{x} \in \partial\Omega.$$ (10)

The problem has two nondimensional parameters, P (scaled pressure) and Q (scaled heat source density). Although one parameter could be eliminated by specifying the time scale $[t]$, we keep both in what follows so that the effects of creep closure and heating remain clear. In addition, the system is invariant to changes in length scale, so $[x]$ is arbitrary.

The assumption of uniform heating across the area of the channel is a significant idealisation. As most heat in turbulent conduit flow is generated in a boundary layer near the walls, an alternative approximation is to take m in (7) to be spatially uniform along the boundary, rather than solving for the temperature distribution in Ω_c. Under such an assumption, a circular conduit is unstable to all modes of perturbation (see section V B). Ultimately, a detailed boundary layer-based model of turbulent heating that takes the wall geometry into account may provide a more realistic model, but that is beyond the scope of this paper.

III.   EXACT SOLUTIONS FROM COMPLEX VARIABLE THEORY

In this section we show that the combined problem (3), (9), (10) admits exact solutions in the form of ellipses whose focal points are fixed in time. We review some relevant results

on the theory of exact solutions for free boundary Stokes flow and Hele–Shaw squeeze flow, which are equivalent to our model of ice flow (3) and melting by uniform heating (9), respectively. In particular, each problem admits a solution where the free boundary is an ellipse that expands or contracts while remaining confocal.

The fact that both of these 'single-phase' problems have confocal ellipses as an exact solution means that they can be combined to produce an exact solution of the full two-phase problem. As seem below, this is because the two terms in the kinematic condition (10) both have the same particular spatial dependence, which ensures that an ellipse with the same focal points is maintained as the boundary evolves.

A.   Stokes flow

First we consider the Stokes flow problem in isolation ($Q = 0$ in (9), so $T \equiv 0$). Exact solutions for the inward creep of viscous fluid have been constructed using conformal mapping[13,14], recently extended to larger classes of solutions by using a Cauchy transform approach[15]. These solutions take the form of rational functions (with time-dependent coefficients) of an auxiliary variable ζ, which map the unit disc $|\zeta| < 1$ in the complex plane, to the fluid region Ω_i, and thus the unit circle $|\zeta| = 1$ to the free boundary $\partial\Omega$. Here we only consider the simplest nontrivial (that is, non-circular) example, which is that given by the mapping

$$z = f(\zeta, t) = c_{-1}(t)\zeta^{-1} + c_{k-1}(t)\zeta^{k-1}. \tag{11}$$

Here k is a positive integer, and the coefficients c_{-1} and c_{k-1} are taken to be real-valued functions of time. The boundary $\partial\Omega$ given by this map is a k-fold symmetric shape, and if $c_{k-1} \ll c_{-1}$, it is equivalent to a circle of radius c_{-1} perturbed by a kth mode sinusoidal perturbation. The two coefficients evolve by[14]

$$\dot{c}_{-1} = -\tfrac{1}{2}Pc_{-1}, \qquad \frac{\mathrm{d}}{\mathrm{d}t}(c_{-1}c_{k-1}) = 0, \tag{12}$$

so that the leading order radius decays exponentially, while any modes of perturbation grow exponentially at a rate independent of the mode number k, hence the boundary is unstable. More generally, (12) implies that, for $k > 2$, the boundary will form cusps at a time before it contracts to a point (see figure 2). The cusp formation corresponds to the critical points
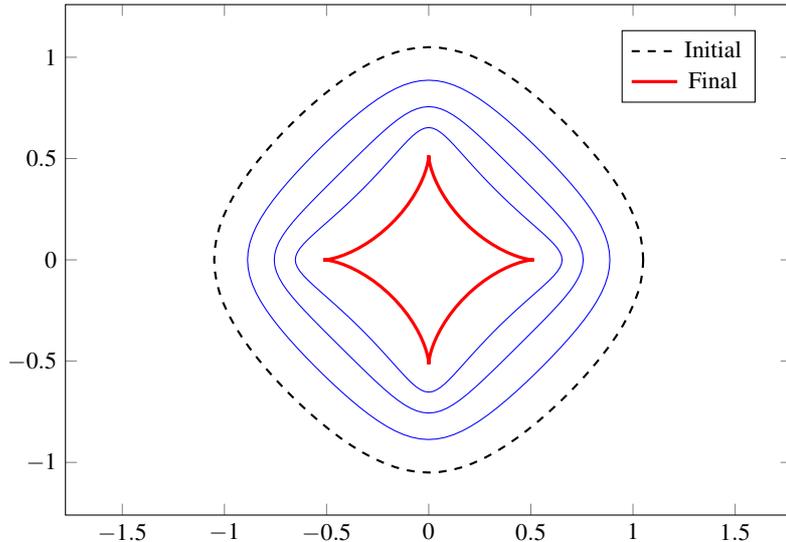
FIG. 2. The exact solution for a contracting cavity in Newtonian Stokes flow given by the conformal mapping (11), with symmetry $k = 4$. As it contracts, the boundary is unstable and develops cusps at a time before the channel contracts to a point.

of the mapping function f (that is, points where $f_\zeta = 0$) intersecting the unit circle. Beyond this time the exact solution is no longer valid, as f is no longer one to one.

A special case is $k = 2$, in which case (11) maps the unit circle exactly to an ellipse with semiaxes $a = c_{-1} + c_1$ and $b = c_{-1} - c_1$. In this case, cusp formation occurs at the same time as extinction. The focal points of an ellipse are at $\pm\sqrt{a^2 - b^2} = \pm 2\sqrt{c_{-1} c_1}$, thus from (12) the focal points are fixed in time. Writing (12) in terms of the evolution of the semi-axes:

$$\dot{a} = -\tfrac{1}{2}Pb, \qquad \dot{b} = -\tfrac{1}{2}Pa. \tag{13}$$

For a circle, $a = b$, and (13) gives exponential decay for the radius, and thus the area. If $a > b$, then b contracts faster than a, becoming zero in finite time.

For reference in the coupled problem, we note that the normal velocity on the boundary of this ellipse (which provides the kinematic boundary condition) is

$$\boldsymbol{u} \cdot \boldsymbol{n} = -\tfrac{1}{2}P\sqrt{\frac{b^2 x^2}{a^2} + \frac{a^2 y^2}{b^2}}. \tag{14}$$

9

B. Heating

Now we consider uniform heating in isolation ($P = 0$ in (3), thus $\boldsymbol{u} \equiv \boldsymbol{0}$). Classes of exact solutions have been constructed to this problem[15,17,18], again using complex variable methods. For example, one can use the following rule regarding the evolution of the *Cauchy transform* $U(z, t)$, a complex valued function that characterizes the boundary $\partial\Omega(t)$:

$$\frac{\partial}{\partial t}\left(e^{-Qt}U(z, t)\right) = 0, \qquad U(z, t) = \frac{1}{2\pi i}\oint_{\partial\Omega(t)}\frac{\overline{z'}}{z - z'}dz', \tag{15}$$

where $z \in \Omega_i$, that is, outside the boundary[18].

Solutions to (15) can be found again in the form of rational, time-dependent conformal mapping functions from the unit disc, but in general these must map to the *interior* of $\partial\Omega$. For instance, substituting the polynomial function

$$z = f(\zeta, t) = c_1(t)\zeta + c_{k+1}(t)\zeta^{k+1} \tag{16}$$

(with, c_1, c_{k+1} real) into (15) gives

$$U(z, t) = \frac{c_1^2 + (k - 1)c_{k+1}^2}{z} + \frac{c_1^{k+1}c_{k+1}}{z^{k-1}}, \tag{17}$$

and so the coefficients evolve according to

$$\frac{d}{dt}(e^{-Qt}(c_1^2 + (k + 1)c_{k+1}^2)) = \frac{d}{dt}(e^{-Qt}c_1^{k+1}c_{k+1}) = 0. \tag{18}$$

As with the exact solution (12), (18) may be used to determine the linear stability of a kth mode perturbed circle by taking $c_{k+1} \ll c_1$. The two results might be combined to give the stability analysis of the coupled problem (we perform an equivalent analysis in section IV A in polar coordinates). However, the boundaries $\partial\Omega$ given by the two conformal maps (11) and (16) do not coincide exactly; thus it is generally impossible to combine the exact solutions of each individual flow problem such that the kinematic condition (10) is satisfied.

The ellipse is an exception. One can show a mapping of the form $z = c_{-1}\zeta^{-1} + c_1\zeta$ exactly satisfies the Cauchy transform formulation (15) of the problem (see appendix A). Somewhat remarkably, a mapping of the same form also satisfies the modified problem when the additional coupling term in the kinematic boundary condition is included in (15). The coupled solution is much simpler to demonstrate in Cartesian coordinates, however. If again

10

$a(t)$ and $b(t)$ are the semi-axes of an ellipse, the following solution to Poisson's equation (9) for the temperature T is well known:

$$T(x, y, t) = \frac{Qa^2b^2}{2(a^2 + b^2)}\left(1 - \frac{x^2}{a^2} - \frac{y^2}{b^2}\right). \tag{19}$$

Noting that a non-unit normal is given by $(bx/a, ay/b)$, in the absence of creep closure the kinematic condition (10) reads

$$\left(\frac{\dot{a}b}{a^2}x^2 + \frac{a\dot{b}}{b^2}y^2\right) \bigg/ \sqrt{\frac{b^2x^2}{a^2} + \frac{a^2y^2}{b^2}} = Q\frac{ab}{a^2 + b^2}\sqrt{\frac{b^2x^2}{a^2} + \frac{a^2y^2}{b^2}}. \tag{20}$$

and matching terms gives the evolution of the semi-axes a and b:

$$\dot{a} = Q\frac{ab^2}{a^2 + b^2}, \qquad \dot{b} = Q\frac{a^2b}{a^2 + b^2}. \tag{21}$$

Again, since the focal points lie at $\pm\sqrt{a^2 - b^2}$, (21) implies that the ellipse remains confocal.

C. The full problem

We now consider the full problem ($Q, P \neq 0$). Re-introducing the normal creep velocity for the ellipse (14) into the kinematic condition (20) we see that the spatial form of the two terms on the right is the same, as alluded to earlier. Matching coefficients again, we have

$$\dot{a} = -\tfrac{1}{2}Pb + Q\frac{ab^2}{a^2 + b^2}, \qquad \dot{b} = -\tfrac{1}{2}Pa + Q\frac{a^2b}{a^2 + b^2}. \tag{22}$$

This coupled system may be written in terms of the evolution of area $S = \pi ab$, and aspect ratio $\alpha = b/a$:

$$\dot{S} = \left(-\tfrac{1}{2}P\frac{1 + \alpha^2}{\alpha} + Q\right)S, \qquad \dot{\alpha} = -(1 - \alpha^2)\left(\tfrac{1}{2}P - Q\frac{\alpha}{1 + \alpha^2}\right). \tag{23}$$

From (23) it is clear that the decrease in area due to creep closure is at its minimum when the channel is a circle ($\alpha = 1$), and increases as the aspect ratio decreases. The end result is that an initially elliptical channel may close in finite time, whereas a circular one can only decay exponentially to zero (as is easily seen by substituting $a = b$ into (22) or $\alpha = 1$ into (23)). In figure 3 we plot the solutions for an exact solution contracting according to (22), showing the distinct behaviours of an initially circular and initially elliptical boundary.

Unlike the circle, which is only steady if $P = Q$, an ellipse has a steady state for any P and Q (given $Q > P$) where the aspect ratio satisfies $\tfrac{1}{2}P(\alpha + \alpha^{-1}) - Q = 0$. However, for
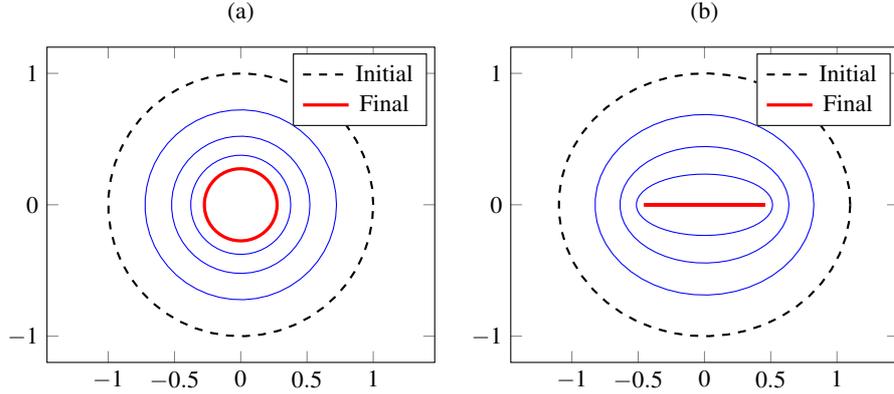
11

FIG. 3. The exact solution (22) for (a) a circle with initial unit radius, and (b) an ellipse with initial semi-axes $a = 1.1$ and $b = 1$. Both solutions are over the same time span, for pressure $P = 2$, and heat source density $Q = 1$. The circle contracts exponentially, while the ellipse contracts to a line in finite time, with aspect ratio decreasing to zero.

fixed P and Q this steady state is unstable, with an elliptical channel (unless initially at the steady state) contracting to a line or growing without bound. In section V we briefly discuss how feedback between the area S and heat density Q (or pressure P), as would appear in a more comprehensive full conduit model, can stabilize the steady states.

As an alternative to (22) or (23), the evolution of the boundary can be written as a single differential equation in elliptic coordinates. Since these coordinates are the natural ones to use for the linear stability analysis in the next section, this result is included below in (42).

IV. STABILITY TO HIGHER ORDER PERTURBATIONS

The above analysis does not indicate whether ellipses are stable to more general perturbations. In this section we derive the stability properties of both circles and ellipses to higher modes, that is, modes that do not correspond to changes in scale or translation, or that follow the leading order solution (22). We use polar and elliptic coordinates, respectively, so that the base state (circle or ellipse) is represented by a constant value of one of the coordinate variables.

For the full problem, we deduce that circles are neutrally stable to second mode perturbations (that is, perturbations that make them ellipses), and stable to all higher modes. The stability of the ellipse depends on its aspect ratio, becoming unstable to a greater number

12

of modes as the aspect ratio decreases.

For simplicity we mostly assume P and Q are such that the base state is at equilibrium; the results may be extended to determine the stability of a time-dependent base state, but in that case greater care must be taken to derive the correct stability criterion, as a base state is only stable if a perturbation decays faster (or grows more slowly) than the base state decays (or grows).

A. The stability of a circle

The linear stability analysis of a circle can be obtained from the existing complex variable solutions (12) and (18), but it is instructive to carry it out using the stress/streamfunction formulation (3), as that approach is required for the ellipse.

Using polar (r, θ) coordinates, let the boundary $\partial\Omega$ be represented by $r = s(\theta, t)$, and take $\partial\Omega$ to be a perturbed circle of radius s_0 by writing $s \sim s_0(t) + \epsilon\tilde{s}(\theta, t)$, for $\epsilon \ll 1$. Other variables also have leading order and correction components: $A \sim A_0(r, t) + \epsilon\tilde{A}(r, \theta, t)$, $\psi \sim \psi_0(\theta, t) + \epsilon\tilde{\psi}(r, \theta, t)$, $T \sim T_0(r, t) + \epsilon\tilde{T}(r, \theta, t)$, and so on. As is standard in the stability analysis of a circular interface, we expect the modes of perturbation (that is, the eigenfunctions of the linear problem for $\tilde{s}$) to be sinusoidal, so we consider a single mode of the form $\tilde{s} = \gamma_k(t) \cos k\theta$, for $k \geq 2$; a more general perturbation can be considered a superposition of such modes. The growth or decay of γ_k indicates the stability of the circle to the kth mode of perturbation.

Both A_0 and $\tilde{A}$ are biharmonic for $r > s_0$, and as the stress boundary condition (3a) is equivalent to $A = A_r = 0$ for $r = s$, they satisfy the linearized conditions

$$A_0 = A_{0r} = 0, \qquad \tilde{A} = 0, \ \tilde{A}_r = -\tilde{s}A_{0rr}, \qquad r = s_0. \tag{24}$$

The far field conditions are $A_{0rr} + r^{-1}A_{0r} \to P$, $\tilde{A}_{rr} + r^{-1}\tilde{A}_r \to 0$. Thus, with the assumed form for $\tilde{s}$, we solve the leading order and correction problems sequentially to obtain:

$$A_0 = \tfrac{1}{4}(r^2 - s_0^2) - \tfrac{1}{2}s_0^2 \log(r/s_0), \qquad \tilde{A} = -\tfrac{1}{2}\gamma_k s_0 \left((r/s_0)^{2-k} - (r/s_0)^{-k}\right) \cos k\theta. \tag{25}$$

To find the leading order and correction to the streamfunction (and hence the normal velocity to substitute into the kinematic condition), we must consider the Goursat representations that corresponds to the above exact solutions. By inspection these are

$$A_0 + i\psi_0 = \tfrac{1}{4}z\overline{z} - \tfrac{1}{2}s_0^2 \log z + \text{const.}, \qquad \tilde{A} + i\tilde{\psi} = -\tfrac{1}{2}\gamma_k s_0^{k-1} z^{1-k}\overline{z} + \tfrac{1}{2}\gamma_k s_0^{k+1} z^{-k} + i \cdot \text{const.}, \tag{26}$$

so the Goursat functions are

$$\phi_0 = \tfrac{1}{4}z, \quad \chi_0 = -\tfrac{1}{2}s_0^2 \log z + \text{const.}, \quad \tilde{\phi} = -\tfrac{1}{2}\gamma_k s_0^{k-1} z^{1-k}, \quad \tilde{\chi} = \tfrac{1}{2}\gamma_k s_0^{k+1} z^{-k} + \text{i·const.} \quad (27)$$

Taking the imaginary part we find ψ_0 and $\tilde{\psi}$:

$$\psi_0 = -\tfrac{1}{2}s_0^2\theta + \text{const.}, \qquad \tilde{\psi} = -\tfrac{1}{2}\gamma_k s_0 \left((r/s_0)^{2-k} - (r/s_0)^{-k}\right)\sin k\theta + \text{const.} \qquad (28)$$

Note that $\tilde{\psi} = 0$ on $r = s_0$, so the streamfunction correction does not contribute to the evolution of modes $k \geq 2$. This interesting result generalizes to the ellipse; see (46).

The leading order temperature T_0 satisfies Poisson's equation, while the correction $\tilde{T}$ satisfies Laplace's equation. The temperature condition on the free boundary implies, after linearisation,

$$T_0 = 0, \qquad \tilde{T} = -\tilde{s}T_{0r}, \qquad r = s_0. \qquad (29)$$

Solving for T_0 and $\tilde{T}$ sequentially, again assuming the form for s_k, gives

$$T_0 = \tfrac{1}{4}Q(s_0^2 - r^2), \qquad \tilde{T} = \tfrac{1}{2}Qs_0\gamma_k(r/s_0)^k \cos k\theta. \qquad (30)$$

The kinematic condition in polar coordinates is $ss_t = (\psi_\theta + s\psi_r s_\theta) - (sT_r - T_\theta s_\theta)$ on $r = s$, the leading and correction terms of which are

$$s_0\dot{s}_0 = \psi_{0\theta} - s_0 T_{0r}, \qquad s_0\tilde{s}_t + \dot{s}_0\tilde{s} = (s_0\tilde{s})_t = \tilde{\psi}_\theta - s_0(\tilde{T}_r + \tilde{s}T_{0rr}) - \tilde{s}T_{0r}, \qquad r = s_0. \quad (31)$$

Substituting in (28) and (30) results in

$$\dot{s}_0 = (-\tfrac{1}{2}P + \tfrac{1}{2}Q)s_0, \qquad (s_0\gamma_k)_t = -(\tfrac{1}{2}k - 1)Qs_0\gamma_k. \qquad (32)$$

Thus a circle is at equilibrium if $P = Q$ (as seen earlier), and all modes of perturbation are stable except the second mode $k = 2$, which is neutrally stable. The second mode perturbs the circle to an ellipse, which is also an exact solution, as described in the previous section.

B.   Stability of time-dependent state

The equations for the leading order and correction to the boundary (32) are still valid if $P \neq Q$, so that the channel is either contracting or expanding. The stability then depends on the perturbation changing more slowly than the base state $s_0(t)$. Combining the two equations in (32) we obtain

$$\frac{\mathrm{d}}{\mathrm{d}t}\log\left|\frac{\gamma_k}{s_0}\right| = \frac{\dot{\gamma}_k}{\gamma_k} - \frac{\dot{s}_0}{s_0} = P - \tfrac{1}{2}kQ. \qquad (33)$$
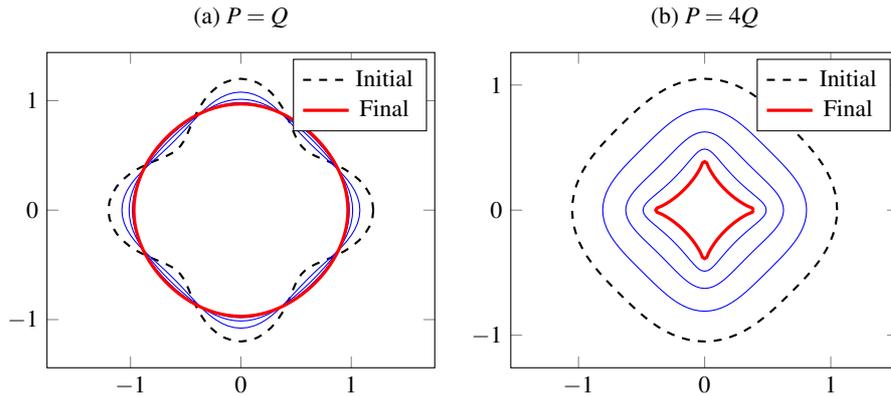
14

FIG. 4. The evolution of a circle perturbed by a fourth mode perturbation: (a) when pressure and heating balance ($Q = P$), the circle is stable. (b) when $P = 4Q$, the circle is unstable according to (33), and cusps form, similar to the exact solution for $Q = 0$ (see figure 2). The solutions are computed using the numerical method outlined in section IV D.

Thus if a circle is contracting ($P > Q$), it is always unstable to second mode perturbations (hence the exact solution of an ellipse of increasing aspect ratio from section III). If P is much greater than Q then higher modes may also be unstable; in figure 4b we plot the numerical solution of a contracting four-fold symmetric channel with $P = 4Q$. Cusps form on the boundary, similar to the exact solution (11) for Stokes flow only ($Q = 0$) shown in figure 2.

C. The stability of an ellipse

Now we carry out a similar process for the ellipse. As the ellipses remain confocal over time, it is convenient to express the solution in elliptical coordinates (ξ, η), where

$$x = C \cosh \xi \cos \eta, \qquad y = C \sinh \xi \sin \eta. \tag{34}$$

The coordinate transformation (34) is the conformal mapping effected by the analytic function $z = C \cosh \zeta$, where $z = x + \mathrm{i}y$ and $\zeta = \xi + \mathrm{i}\eta$, which maps a semi-infinite strip ($\xi > 0$, $0 < \eta < 2\pi$) to the plane. Any function that is continuous in the physical plane must be periodic in η and even around $\xi = 0$, if defined there. The Goursat relation between stress- and streamfunctions is now

$$A(\xi, \eta) + \mathrm{i}\psi(\xi, \eta) = \phi(\zeta) \cosh \overline{\zeta} + \chi(\zeta). \tag{35}$$
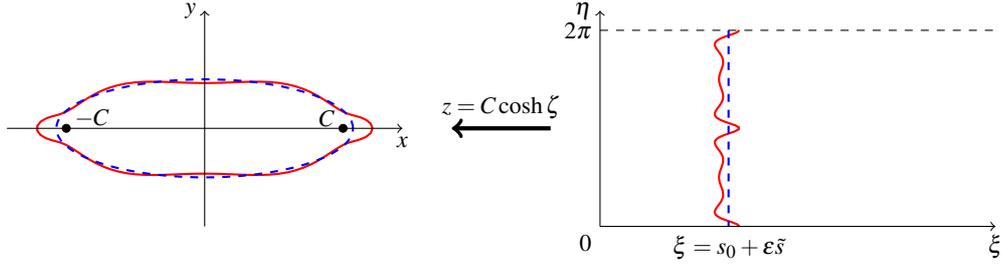
15

FIG. 5. The conformal mapping from elliptic coordinate system $\zeta = \xi + i\eta$ to the physcial plane $z = x + iy$. A perturbation of the form (47) is largest at the ends of the ellipse in the physical plane (a sixth mode perturbation $\tilde{s}_6^e$ is pictured).

The free boundary $\partial\Omega$ is represented by $\xi = s(\eta, t)$; if $s = s_0(t)$ is independent of η, then the boundary is an ellipse with focal points at $\pm C$.

In converting to elliptic coordinates the square scale factor h^2 is important:

$$h^2(\xi, \eta) = \left|\frac{dz}{d\zeta}\right|^2 = \tfrac{1}{2}C^2(\cosh 2\xi - \cos 2\eta). \tag{36}$$

The Laplacian is $\nabla^2 = h^{-2}(\partial^2/\partial\xi^2 + \partial^2/\partial\eta^2)$, while the kinematic condition is now

$$h^2 s_t = (\psi_\eta + \psi_\xi s_\eta) - (T_\xi - T_\eta s_\eta), \qquad \xi = s(\eta, t). \tag{37}$$

It is straightforward to show that the solutions for the stress function and the temperature for an elliptical boundary $s = s_0(t)$ are

$$A_0 = \tfrac{1}{8}PC^2(\sinh 2\xi - 2\xi \cosh 2s_0) + \text{const.} \tag{38}$$

$$T_0 = \tfrac{1}{8}QC^2 \operatorname{sech} 2s_0(\cosh 2s_0 - \cosh 2\xi)(\cosh 2s_0 - \cos 2\eta). \tag{39}$$

By inspection, the corresponding Goursat functions are

$$\phi_0 = \tfrac{1}{4}PC^2 \sinh \zeta, \qquad \chi_0 = -\tfrac{1}{4}PC^2\zeta \cosh 2s_0 + \text{const.}, \tag{40}$$

giving a streamfunction

$$\psi_0 = -\tfrac{1}{8}PC^2(2\eta \cosh 2s_0 - \sin 2\eta) + \text{const.} \tag{41}$$

Now differentiating and substituting into the kinematic condition, each term has a factor of $h^2(s_0, \eta)$ which cancels, leaving an ordinary differential equation for s_0:

$$\dot{s}_0(t) = -\tfrac{1}{2}P + \tfrac{1}{2}Q \tanh 2s_0. \tag{42}$$

16

This expressions is equivalent to the previously derived exact solution (22) or (23).

The calculation of stability of an ellipse is a greater technical challenge than that for a circle, as we cannot expect modes of perturbation to be sinusoidal functions of η, but surprisingly the linearized correction problem can still be solved exactly. As before, define order ϵ correction terms to each variable: $s = s_0 + \epsilon\tilde{s}$, $A = A_0 + \epsilon\tilde{A}$, $\psi = \psi_0 + \epsilon\tilde{\psi}$, and $T = T_0 + \epsilon\tilde{T}$. By substituting into the governing equations and boundary conditions, and taking terms to $\mathcal{O}(\epsilon)$, we obtain a linear problem for the correction terms. The correction to the stress satisfies

$$\nabla^4 \tilde{A} = 0, \qquad\qquad \xi > s_0, \qquad (43a)$$

$$\tilde{A} = 0, \quad \tilde{A}_\xi = -\tilde{s}A_{0\xi\xi} = -\tfrac{1}{2}\tilde{s}PC^2 \sinh 2s_0, \qquad\qquad \xi = s_0, \qquad (43b)$$

$$\nabla^2 \tilde{A} \to \infty, \qquad\qquad \xi \to \infty, \qquad (43c)$$

while the problem for the temperature correction term is

$$\nabla^2 \tilde{T} = 0, \qquad\qquad \xi < s_0, \qquad (44a)$$

$$\tilde{T} = -\tilde{s}T_{0\xi} = \tfrac{1}{2}h^2 \tilde{s}\, Q \tanh 2s_0, \qquad\qquad \xi = s_0, \qquad (44b)$$

$$\tilde{T}_\xi = 0, \qquad\qquad \xi = 0. \qquad (44c)$$

The correction to the kinematic condition (37) may be written as a linear equation

$$(h^2 \tilde{s})_t = \tilde{\psi}_\eta - (\tilde{T}_\xi + \tilde{s}T_{0\xi\xi}) = \mathcal{L}(h^2 \tilde{s}), \qquad \xi = s_0, \qquad (45)$$

where the linear dependence of the right hand side on $\tilde{s}$ comes from solving the correction problems (43) and (44). The correction to the streamfunction $\tilde{\psi}$ is again related to $\tilde{A}$ through the Goursat relation (35). In fact, given the problem (43) for $\tilde{A}$, the linear operation mapping $\tilde{s}$ to ψ_η is quite degenerate; we derive the following result in appendix B:

$$\tilde{\psi}_\eta = \tfrac{1}{4}PC^4 \sinh^2 2s_0 \left(\left\langle \frac{\tilde{s}}{h^2} \right\rangle + \left\langle \frac{\tilde{s}}{h^2}\cos\eta \right\rangle \cos\eta + \left\langle \frac{\tilde{s}}{h^2}\sin\eta \right\rangle \sin\eta \right), \qquad \xi = s_0, \quad (46)$$

where $\langle\cdot\rangle$ represents the average over $\eta \in [0, 2\pi]$.

The form of (45) and (46) suggests an exact solution as a series

$$\tilde{s}(\eta, t) = \tilde{s}_0^{\mathrm{e}}(\eta, t) + \sum_{k=1}^{\infty} \tilde{s}_k^{\mathrm{e}}(\eta, t) + \tilde{s}_k^{\mathrm{o}}(\eta, t), \quad \tilde{s}_k^{\mathrm{e}} = \gamma_k^{\mathrm{e}}(t)\frac{\cos k\eta}{h(s_0, \eta)^2}, \quad \tilde{s}_k^{\mathrm{o}} = \gamma_k^{\mathrm{o}}(t)\frac{\sin k\eta}{h(s_0, \eta)^2}. \quad (47)$$

(Unlike the circle, it is important to distinguish sine and cosine terms here as the ellipse is not rotationally invariant.) The $k = 0$ and $k = 1$ terms in (47) correspond to changes in

17

scale and translation, with respect to which the problem is invariant, so we focus on the higher terms $k \geq 2$. However, it is important to note that higher order terms do induce a change in the $k = 0, 1$ terms through (46), so they cannot be considered modes in the normal sense. If the base state s_0 is constant, a true mode (that is, an eigenfunction of $\mathcal{L}$ in (45)) can be constructed by adding on an appropriate low order term to $\tilde{s}_k^{\mathrm{e}}$ or $\tilde{s}_k^{\mathrm{o}}$. This is not the case when $\dot{s}_0 \neq 0$, so for the sake of simplicity we consider only the fate of the higher order terms themselves, ignoring their contribution to the $k = 0, 1$ terms.

The degeneracy of (46) means that the evolution of $\tilde{\gamma}_k$ for $k \geq 2$ depends only on the solution to the heating problem (44). Given a single cosine term $\tilde{s}_k^{\mathrm{e}}$ we find

$$\tilde{T} = \tfrac{1}{2} Q \tanh 2s_0 \frac{\cosh k\xi}{\cosh k s_0} \gamma_k^{\mathrm{e}} \cos k\eta, \tag{48}$$

thus from (45) it follows

$$\dot{\gamma}_k^{\mathrm{e}} = -\tfrac{1}{2} Q \gamma_k^{\mathrm{e}} (k \tanh 2s_0 \tanh k s_0 - 2) \tag{49}$$

where $k \geq 2$. For sine terms $\tilde{s}_k^{\mathrm{o}}$ the result is

$$\dot{\gamma}_k^{\mathrm{o}} = -\tfrac{1}{2} Q \gamma_k^{\mathrm{o}} (k \tanh 2s_0 \coth k s_0 - 2). \tag{50}$$

For $k = 2$, it is easy to check that a cosine mode $\tilde{s}_2^{\mathrm{e}}$ evolving by (49) (combined with the appropriate $k = 0$ term) is equivalent to a perturbation along the exact base solution (42). Also, (50) implies the second sine perturbation $\tilde{s}_2^{\mathrm{o}}$, which corresponds to a rotation of the ellipse, is neutrally stable.

While the series solution (47) holds for time-dependent s_0, for simplicity we will consider the case where the leading order solution to be at steady state; from (42) this occurs when $P = Q \tanh 2s_0$. In this case, the only time dependence is in the coefficient γ_k, so stability is determined by the sign of $\dot{\gamma}_k^{\mathrm{e}}$ and $\dot{\gamma}_k^{\mathrm{o}}$ from (49) and (50), respectively.

From (50) it follows that $\dot{\gamma}_k^{\mathrm{o}}$ is negative for all $s_0 > 0$, $k \geq 3$ (recall $k = 2$ is a neutrally stable rotation) so the sine terms are stable for all steady ellipses. A cosine term, however, will be unstable when s_0 is less than a critical value $s_0^*(k)$, given by the right hand side of (49) equal to zero (note $s_0 = \tanh \alpha \sim \alpha$ for small s_0, where α is the aspect ratio). The first couple of these (not counting $k = 2$) can be calculated explicitly:

$$s_0^*(3) = \log(\tfrac{1}{2}(\sqrt{5} + 1)) \approx 0.48, \qquad s_0^*(4) = \tfrac{1}{2} \log(\tfrac{1}{2}(\sqrt{6} + \sqrt{2})) \approx 0.33, \tag{51}$$

with higher $s_0^*(k)$ decreasing asymptotically to zero as $k \to \infty$.

18

D. Numerical method

To illustrate the above stability analysis we construct numerical solutions to the coupled problem (1), (9), (10). The numerical method we use is a boundary integral formulation in physical $(\boldsymbol{u}, p, T)$ variables. The free boundary is discretized with N nodes, with the normal $\boldsymbol{n}$ to the boundary computed using centred finite differences. The ice velocity $\boldsymbol{u}$ and normal derivative of the temperature $\boldsymbol{\nabla} T \cdot \boldsymbol{n}$ are both computed by solving discretized versions of the singular linear integral equations (that is, linear matrix equations)[23,24], and then the node positions are moved according to (10) using an explicit ODE solver (`ode45` in Matlab). Due to the stress-free boundary condition (1b), the equation for $\boldsymbol{u}$ only includes the double layer potential, and so possesses only a removable singularity at the reference point, but does not uniquely determine $\boldsymbol{u}$. To close the problem we include an additional equation for the pressure using the Lorentz reciprocal theorem[25], with the origin (assumed to be interior to the boundary) as a reference point.

As temperature T satisfies Poisson's equation (9) we subtract off a particular solution (that is, $\hat{T} = T - \frac{1}{4}Q(x^2 + y^2)$) and use the boundary integral formulation for Laplace's equation. We deal with the logarithmic singularity at the reference point by approximating the free boundary and the temperature derivative as piecewise linear, and exactly calculating the improper integrals on the two line segments adjacent to the singularity.

In figure 6 we show the results of two computations. In both cases the pressure P and heat source density Q are set such that the initial condition is a perturbation of a steady ellipse. In figure 6(a) the initial condition is a large perturbation, symmetric in both axes, from an ellipse of moderately large aspect ratio. The free boundary tends towards an ellipse. In figure (6)b the initial condition is a smaller perturbation (again symmetric in both axes) of an ellipse with aspect ratio 0.2. This aspect ratio is less than the critical value $s_0^*(4)$ (51) at which the fourth mode $\tilde{s}_4^{\mathrm{e}}$ becomes unstable. The result is that the perturbation grows, most noticeably at the end points, where cusps (pointing into the ice) appear to form in finite time. Since such cusp formation is the generic behaviour of contracting Stokes flow without the inner heating (see figure 2), the same behaviour here seems quite reasonable.
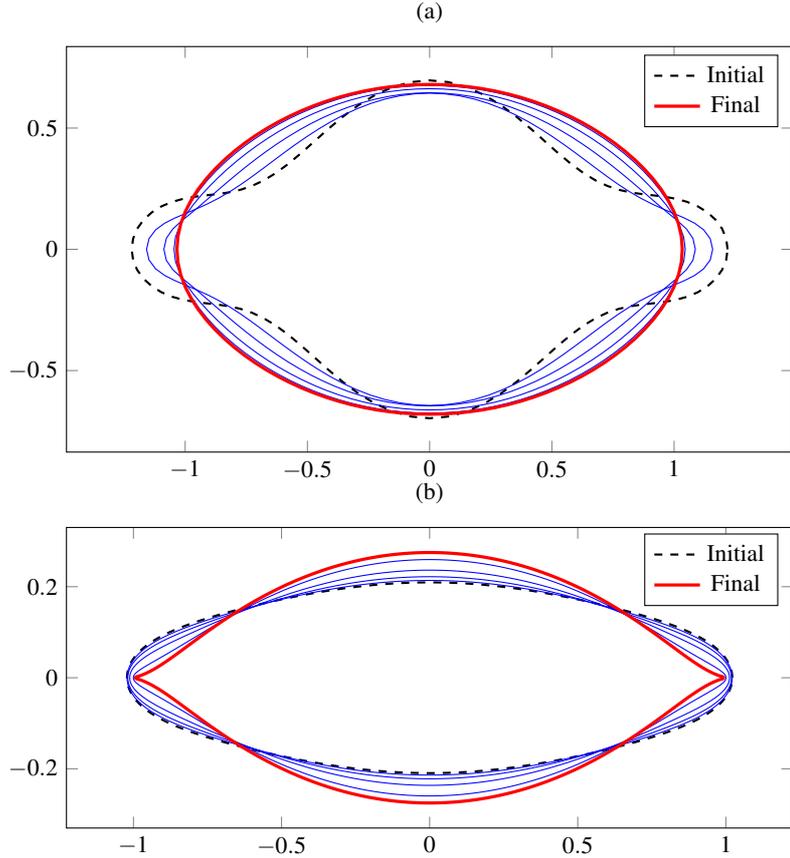
FIG. 6. Numerical solutions to the coupled creep closure/melting problem (1), (9), (10) using the method outlined in section IV D: (a) a sufficiently "fat" shape tends to an ellipse; (b) a shape with small aspect ratio, even if initially close to an ellipse, forms outward-pointing cusps at the ends where curvature is greatest.

V. DISCUSSION AND EXTENSIONS

In this section we consider some extensions to the idealized theory from sections and III and IV. That theory has shown that assuming Newtonian creep for the ice flow and a uniform heat source within the conduit, the free boundary can expand and contract as a series of confocal ellipses. Here, we firstly consider the family of possible steady states; secondly we consider an alternative melting model; and thirdly we consider the implications of non-Newtonian creep.

A.   Feedbacks between cross-sectional area, source heating, and pressure

The exact elliptical solution in (23), expressed in terms of cross-sectional area S and aspect ratio α, can be described by trajectories in the (S,α) phase plane, as in figure 7(a). There is a continuous family of steady states given by

$$Q - \tfrac{1}{2}P\frac{1+\alpha^2}{\alpha} \equiv F(\alpha) = 0, \tag{52}$$

which determines a line of constant α intersecting each trajectory. As is clear from the directions of the trajectories in figure 7, this steady state is unstable; more circular ellipses ($F > 0$) grow indefinitely, while thinner ellipses ($F < 0$) will contract to a line in finite time, as in figure 3.

So far we have taken effective pressure P and heat source density Q to be constant. However, in more comprehensive models of a meltwater conduit, there is likely to be a feedback of the size and shape of the cross-section on both of these two parameters, due to the internal hydrodynamics. Our exact solution (23) is still valid if P and Q change over time, and we can therefore consider making them functions of S, for instance. The steady states are still given by (52) but now with $F = F(S, \alpha)$. The equilibrium line on the phase plane depends on the form of P and Q; if Q is decreasing (or P is increasing) in S, the effect may be to stabilize the family of steady states.

As a simple example, suppose we required that the total energy source QS (per unit length of the conduit) be constant. Then $Q \propto 1/S$ (note that this introduces a length scale into the problem, which can be used to set the constant of proportionality to unity). The resulting family of steady states is depicted on the phase plane in figure 7(b); the steady states are now stable.

On the other hand, the standard circular-cavity models often take the overall heating rate due to turbulent dissipation to be proportional to S^α, with $\alpha > 1$ and the proportionality depending on the potential gradient and the wall roughness[6]; this suggests the uniform heat source density should vary in proportion to $S^{\alpha-1}$, and makes the steady state even more unstable to perturbations. Such a runaway melting instability is well known to glaciologists, and is thought to be responsible for enormous subglacial floods[27]; it can be stabilized be a compensating increase in the effective pressure as S grows.
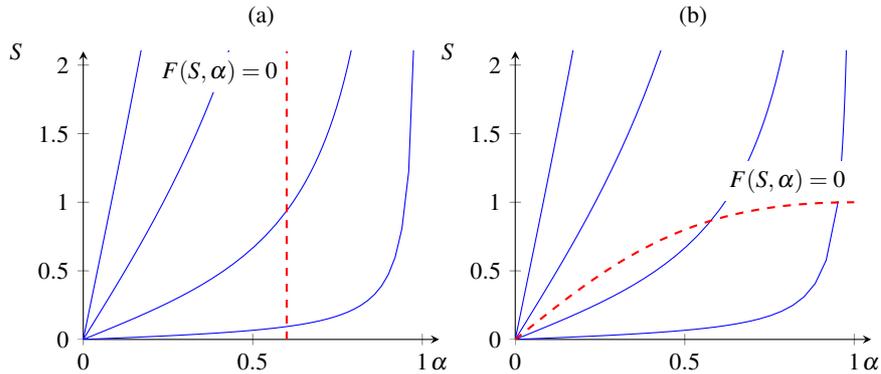
FIG. 7. Trajectories of elliptical cavities in the space of cross-sectional area S and aspect ratio α. (a) when the heat source density Q is fixed, the steady state given by (52) is unstable. (b) if heat source $Q = 1/S$, this can stabilize the ellipse with respect to perturbations along the trajectory.

B.   A uniform melting model

If the heating is caused by viscous dissipation in turbulent flow, it is likely that most heat is produced in a narrow boundary layer near the channel wall, as opposed to uniformly across the channel. The existing circular-conduit models effectively assume that all heat is produced at the channel wall and goes directly into melting at the interface. If we adopt the same assumption in our model, there is no internal heat problem to solve and the kinematic condition (10) is simply replaced by

$$v_n = \boldsymbol{u} \cdot \boldsymbol{n} + M(t) \tag{53}$$

where M is the uniform melt rate at the perimeter.

In this case an ellipse is no longer an exact solution (an initially elliptical interface will immediately evolve into a different shape). The stability analysis for a circle is still applicable, however. For a kth-mode perturbed circle $r = s_0(t) + \epsilon\gamma_k(t)\cos k(\theta)$, the leading order and correction give

$$\dot{s}_0 = -\tfrac{1}{2}P + M, \qquad (s_0\gamma_k)_t = M\gamma_k \tag{54}$$

(compare with (32)). Thus if the circle is at steady state ($M = \tfrac{1}{2}P$), all modes of perturbation grow at a rate $\dot{\gamma}_k = \tfrac{1}{2}P\gamma_k$.

The numerical method described in section IV D is easily adapted to the new kinematic condition (53). In figure 8 we display the results of an initially circular interface with a fourth mode perturbation. The unstable boundary develops inward-pointing corners, instead
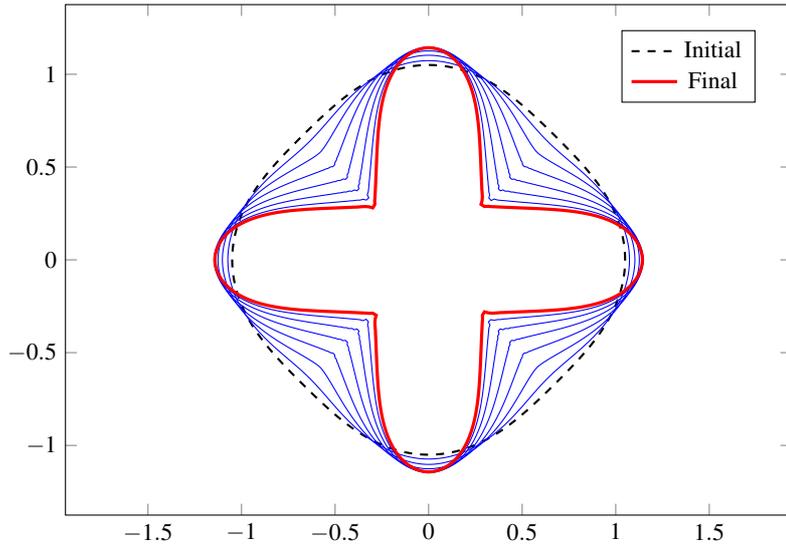
FIG. 8. A four-fold symmetric channel with melting at the edge, evolving according to (53). A circular channel is unstable as predicted by (54), and the boundary develops inward-pointing corners. The boundary does not appear to be approaching a steady state.

of outward-pointing cusps, as occurs for the Stokes flow problem without melting[14]. The corners continue to propagate inwards, and the boundary does not appear to approach a steady state.

To gain a better understanding of the morphology of the conduit walls, a more realistic model of heating and heat transfer in the boundary layer near the wall is probably needed. In such a model the distribution of melting along the interface would be almost uniform but somehow related to the local geometry of the boundary (the local curvature, for instance). Coupled with the inward creep of ice, this could lead to the existence of a stable, non-circular cross section. A similar model of turbulent boundary layer heating is also needed to model the rough scalloped walls that develop in real meltwater conduits. Although such scalloping also occurs in situations where creep closure is not applicable, our results concerning the instability of the free-boundary in creeping flow raise intriguing questions about the interaction between turbulent flow and ice deformation. We leave these questions for future work.

C. A non-Newtonian flow model

The theory of exact solutions for free boundary Stokes flow described in section III A requires that the fluid be Newtonian. It is more accurate to model creeping ice as a shear-thinning power law fluid with viscous stress tensor $\boldsymbol{\tau} = \mathcal{A}|D|^{n-1}\boldsymbol{D}$, where the power-law exponent $n \approx \frac{1}{3}$ (note the reciprocal of n is more commonly used in the glaciology literature where strain rate is defined as a function of stress; we follow the usual opposite convention from fluid mechanics). Given such a rheology, the only exact solutions known are ones with circular symmetry, such as those considered by Nye[5] (the methods used previously can no longer be used to find other exact solutions). However, the stability analysis of the contracting circle to small perturbations (that is, the generalisation of section IV A) is still tractable. We summarize this analysis below, disregarding the effect of melting for simplicity; the effect of melting can be subsequently included in the kinematic condition if desired, and will have a similar stabilizing effect as described earlier.

Again we use polar coordinates and write the free boundary as $r = s_0(t) + \epsilon\gamma_k(t)\cos k\theta$. While a stress function formulation is no longer possible, the $\mathcal{O}(\epsilon)$ linear correction problem may be solved in terms of the primary variables (that is, velocity $\boldsymbol{u} = u\boldsymbol{e}_r + v\boldsymbol{e}_\theta$ and pressure p). We look for correction terms of the form

$$\tilde{u} = (U_1 r^{a_1(k)} + U_2 r^{a_2(k)})\cos k\theta,$$
$$\tilde{v} = (V_1 r^{a_1(k)} + V_2 r^{a_2(k)})\sin k\theta, \tag{55}$$
$$\tilde{p} = (P_1 r^{b_1(k)} + P_2 r^{b_2(k)})\cos k\theta.$$

Closed form expressions for the coefficients and exponents are determined from the governing equation and boundary conditions; the expressions are somewhat unwieldy and are deferred to appendix C. For shear thinning flow $n < 1$, the exponents a_j and b_j may be complex, implying that the velocity and pressure may oscillate outward from a perturbed cavity. In figure 9a we plot the exponents for the second mode $k = 2$ over different n; the exponents become complex for $n \lesssim 0.8$. The value below which exponents are complex tends asymptotically to $n = 1$ as mode number $k \to \infty$.

From the kinematic condition we derive formulae for the evolution of the leading order radius s_0 and the kth mode magnitude γ_k:

$$\dot{s}_0 = \left(\frac{np^\infty}{\mathcal{A}}\right)^{1/n} s_0, \qquad \dot{\gamma}_k = \left(\frac{np^\infty}{\mathcal{A}}\right)^{1/n} C_k(n)\gamma_k, \tag{56}$$

24

The first of these is the result obtained by Nye[5] for a circular cavity, while the kth mode nondimensional growth rate C_k (defined in the appendix) depends only on the power-law exponent n and mode number k. In figure 9b we plot these values over n for various k. While all modes are unstable for any n, in a shear thinning fluid the lower modes grow more slowly than the higher ones. As $k \to \infty$, the growth rate is bounded by the Newtonian growth rate $C_k = 1$, that is, high mode perturbations asymptotically grow at the same rate that the leading order radius contracts. Thus we generically expect cusp formation still to occur for the contracting cavity in shear-thinning flow, as for the Newtonian case.

It would be worthwhile using a numerical scheme to test the predictions of this linear stability analysis, including the oscillations in velocity and pressure due to the complex values of the exponents a_j. The boundary integral method we employed in section IV D does not extend to non-Newtonian fluids, but finite elements might be used. In addition, while not relevant to ice flow, the stability of contracting cavities in shear thickening fluid ($n > 1$) is also worth further exploration. Although our linear stability analysis formally extends to $n > 1$, in this regime one of the exponents in the velocity, a_j, is larger than -1 (see figure 9). Since the leading order velocity $u_0 \propto 1/r$, the asymptotic series in ϵ will not be uniformly valid as radius $r \to \infty$. We leave this issue for future study.

D. Summary and Conclusion

We have applied techniques from the theory of two-dimensional free-boundary problems to understand the cross-sectional evolution of a conduit that contracts due to creep closure, and expands due to melting of the walls. Assuming Newtonian creep for the ice and a uniform heat source in the water, an exact solution exists in which the boundary contracts or expands as a series of ellipses with fixed focal points. A key implication of this theory is that the rate of conduit closure, given by (23), depends upon the aspect ratio. The closure rate is larger for smaller aspect ratios, and as the aspect ratio shrinks to zero, the cross-sectional area shrinks to zero in finite time. For a given total energy source, a conduit with smaller aspect ratio therefore requires a smaller effective pressure to be in steady state.

We analysed the stability of the circular and elliptical solutions, and constructed numerical solutions using boundary integral techniques. These show that for fat enough ellipses, uniform heating acts to stabilize perturbations of the interface, but for small aspect ratio
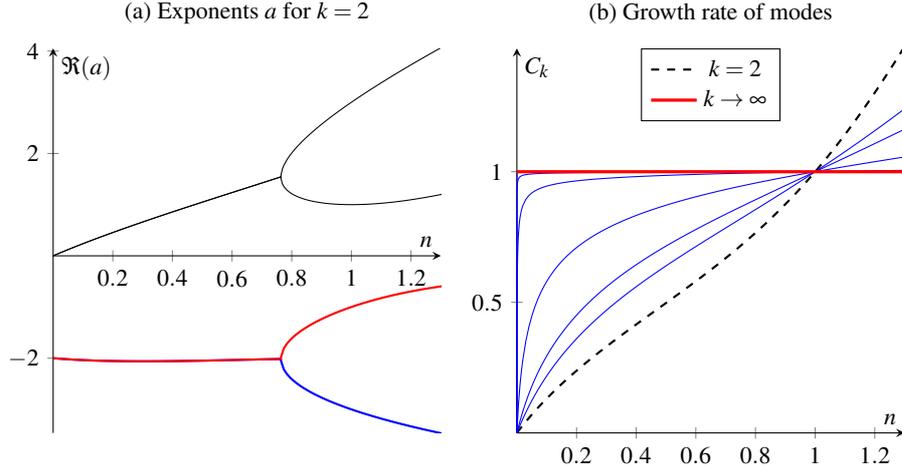
25

(a) Exponents a for $k = 2$

(b) Growth rate of modes

FIG. 9. Results of the linear stability analysis for a shear thinning fluid ($n < 1$): (a) the four exponents a in the ansatz (55), for $k = 2$ (see (C2)). The two a_j with negative real parts are the relevant ones for fluid flow outside a perturbed circle. For sufficiently small n, the two exponents are complex conjugate, implying that physical variables (velocity u, pressure p) exhibit damped oscillations in r. (b) the nondimensional growth rate C_k of kth mode perturbations, against power law exponent n. The effect of shear thinning is to reduce the instability in lower order modes, while as $k \to \infty$, the growth rate approaches the Newtonian growth rate.

ellipses, the interface is unstable. This instability may help explain the convoluted shapes of many englacial conduits[28]. Although derived from an idealized system of equations, we believe the behaviour of these solutions qualitatively captures much of the behaviour of the real physical system. Similar behaviour is seen in numerical computations that employ different assumptions of ice rheology and melting[10], and the suggestion that shallow aspect ratio ellipses close more quickly was previously used to explain higher observed water pressures than predicted by the circular-conduit theory[8]. Extensions to the current theory that account for non-Newtonian behaviour and uniform melting, outlined earlier in this section, do not significantly alter the results. The most significant difference is that uniform wall melting is ineffective at stabilizing the interface to perturbations, and this suggests that a more detailed analysis of the turbulent heat transfer problem would be a worthy case for further study.

ACKNOWLEDGMENTS

Appendix A: Cauchy Transform for squeeze flow (Poisson equation) with elliptic boundary

The external Cauchy transform U of a boundary evolving according to Hele–Shaw squeeze flow, with plate separation $B(t)$, satisfies[18]

$$\frac{\partial}{\partial t}\left[B(t)U(z,t)\right] = 0, \qquad U(z,t) = \frac{1}{2\pi i}\oint_{\partial\Omega}\frac{\overline{z}'}{z-z'}dz', \tag{A1}$$

where z is outside $\partial\Omega$. An ellipse is the image of the unit circle under $z = c_{-1}\zeta^{-1} + c_1\zeta$, thus

$$U(z(\zeta,t),t) = -\frac{1}{2\pi i}\oint_{|\zeta|=1}\frac{(c_{-1}\zeta' + c_1\zeta'^{-1})(-c_{-1}\zeta'^{-2} + c_1)}{c_{-1}\zeta^{-1} + c_1\zeta - c_{-1}\zeta'^{-1} - c_1\zeta'}d\zeta'$$

Here ζ is taken to be the preimage of z that is in the unit disc (there is another one outside). The coefficients c_{-1} and c_1 are taken to be real and positive functions of t (this changes the orientation of the curve, which introduces the minus sign). The integrand has two poles at $\zeta' = 0, \zeta$, with

$$\operatorname*{Res}_{\zeta'=0}[\text{integrand}] = \frac{c_{-1}}{c_1}\left(\frac{c_{-1}}{\zeta} + c_1\zeta\right), \qquad \operatorname*{Res}_{\zeta'=\zeta}[\text{integrand}] = -\left(c_{-1}\zeta + \frac{c_1}{\zeta}\right),$$

so the integral can be computed easily enough:

$$U(z,t) = \left(c_{-1} - \frac{c_1^2}{c_{-1}}\right)\zeta = \frac{c_{-1}^2 - c_1^2}{2c_{-1}c_1 z}\left(1 - \sqrt{1 - \frac{4c_{-1}c_1}{z^2}}\right).$$

Changing back to z is necessary as it is the time derivative holding z constant that vanishes in (A1). A constant term $-Q$ in Poisson's equation corresponds to $B(t) = e^{-Qt}$, thus (A1) is satisfied given

$$\frac{d}{dt}\left((c_{-1}^2 - c_1^2)e^{-Qt}\right) = 0, \qquad \frac{d}{dt}(c_{-1}c_1) = 0.$$

These two equations give the exponential increase in area and fixed focal points, respectively.

One might be concerned that the functional form of this Cauchy transform is altered by the additional term in the kinematic condition when coupled to the external viscous flow

problem. That coupling generates an extra term in (A1), but it can be shown that for the particular case of an ellipse this has the same functional form (in z) and that it gives rise to a modification of the evolution equations, as in (22). Similarly, one can construct the Cauchy transform of the exterior domain[29], and find that the additional terms from the full kinematic boundary condition have the same functional form for the exact solution.

Appendix B: The correction to the streamfunction

Here we provide detail on the derivation of the equation (46) for the correction to the derivative of the streamfunction $\tilde{\psi}$, given the problem (43) for the correction to the stress function. The degeneracy of (46) is due to the free boundary condition $\tilde{A}(s_0, \eta) = 0$, and the Goursat relation (35) that relates $\tilde{A}$ and $\tilde{\psi}$ through the corrections to the Goursat functions, $\tilde{\phi}$ and $\tilde{\chi}$:

$$\tilde{A} + i\tilde{\psi} = \tilde{\phi}(\zeta) \cosh \overline{\zeta} + \tilde{\chi}(\zeta).$$

Noting that $\overline{\zeta} = \zeta - 2s_0$ on $\xi = s_0$, define the complex-valued functions

$$F(\zeta) = \tilde{\phi}(\zeta) \cosh(\zeta - 2s_0) + \tilde{\chi}, \qquad G(\zeta) = F_\zeta(\zeta) - 2\tilde{\phi}(\zeta) \sinh(\zeta - 2s_0),$$

so that F and G are analytic for $\xi > s_0$, while on $\xi = s_0$, $F(\zeta) = \tilde{A} + i\tilde{\psi}$ and $G(\zeta) = \tilde{A}_\xi + i\tilde{\psi}_\xi$. The corrections to pressure and velocity must vanish in the far field, which determines the behaviour of ϕ and χ for large ξ (see Tanveer & Vasconcelos[14]):

$$\tilde{\phi} \sim \phi_\infty \in \mathbb{C}, \qquad \frac{d\tilde{\chi}}{dz} \sim \frac{\overline{\phi_\infty}}{C} \Rightarrow \tilde{\chi} \sim \int \frac{\overline{\phi_\infty}}{C} \frac{dz}{d\zeta} d\zeta \sim \frac{\overline{\phi_\infty}}{2} e^\zeta, \qquad \xi \to \infty.$$

(Note that a factor of C was incorporated into ϕ in (35)). The complex constant ϕ_∞ is determined below. The far field behaviour of F and G is then

$$F \sim \left(\tfrac{1}{2}\phi_\infty e^{-2s_0} + \tfrac{1}{2}\overline{\phi_\infty}\right) e^\zeta, \qquad G \sim \left(-\tfrac{1}{2}\phi_\infty e^{-2s_0} + \tfrac{1}{2}\overline{\phi_\infty}\right) e^\zeta, \qquad \xi \to \infty.$$

In addition, for all physical variables to be single-valued, G and F_ζ (but not necessarily F) must be periodic with period $2\pi i$. Given $\Re(F) = \tilde{A} = 0$ on $\xi = s_0$, the form of F is uniquely determined up to a few constants:

$$F(\zeta) = \overline{\phi_\infty} \sinh \zeta - \phi_\infty \sinh(2s_0 - \zeta) + b(\zeta - s_0) + ic,$$

28

where b and c are additional free constants. Thus the correction to the streamfunction only has the terms

$$\tilde{\psi}_\eta(s_0) = \Im(F)_\eta = b + 2\cosh s_0 \phi'_\infty \cos\eta + 2\sinh s_0 \phi''_\infty \sin\eta$$

where we write $\phi_\infty = \phi'_\infty + i\phi''_\infty$. The constants b, ϕ'_∞ and ϕ''_∞ are determined from the condition $\Re(G) = \tilde{A}_\xi$ on $\xi = s_0$, which allows them to be computed in terms of integral quantities of $\tilde{A}_\xi$, and thus $\tilde{s}$. Given

$$G(\zeta) = \overline{\phi_\infty}\cosh\zeta + \phi_\infty\cosh(\zeta - 2s_0) + b - 2\tilde{\phi}(\zeta)\sinh(\zeta - 2s_0),$$

the following integrals are computed using complex residues:

$$C^2 \int_0^{2\pi} \frac{\tilde{A}_\xi}{h^2}\,\mathrm{d}\eta = -\Im\left(\oint_\Gamma \frac{G(\zeta)}{\sinh\zeta\sinh(2s_0 - \zeta)}\,\mathrm{d}\zeta\right) = \frac{4\pi b}{\sinh 2s_0}$$

$$C^2 \int_0^{2\pi} \frac{\tilde{A}_\xi}{h^2}\cos\eta\,\mathrm{d}\eta = -\Im\left(\oint_\Gamma \frac{G(\zeta)\cosh(\zeta - s_0)}{\sinh\zeta\sinh(2s_0 - \zeta)}\,\mathrm{d}\zeta\right) - 4\pi\phi'_\infty\sinh s_0 = \frac{4\pi\phi'_\infty}{\sinh s_0}$$

$$-C^2 \int_0^{2\pi} \frac{\tilde{A}_\xi}{h^2}\sin\eta\,\mathrm{d}\eta = -\Re\left(\oint_\Gamma \frac{G(\zeta)\sinh(\zeta - s_0)}{\sinh\zeta\sinh(2s_0 - \zeta)}\,\mathrm{d}\zeta\right) + 4\pi\phi''\cosh s_0 = \frac{4\pi\phi''_\infty}{\cosh s_0}.$$

Here Γ is the boundary of the semi-infinite strip $\xi > s_0$, $-\delta < \eta < 2\pi - \delta$, and the integrand in each case has two simple poles at $\zeta = 2s_0$ and $\zeta = 2s_0 + i\pi$. In the latter two cases, the integrand approaches a non-zero value as $\xi \to \infty$ so the integral there is subtracted off. Rearranging for the constants, using the stress condition (43b) and substituting into $\tilde{\psi}_\eta$ we obtain the result (46):

$$\tilde{\psi}_\eta(s_0) = \frac{PC^4\sinh^2 2s_0}{4}\left(\left\langle\frac{\tilde{s}}{h^2}\right\rangle + \left\langle\frac{\tilde{s}}{h^2}\cos\eta\right\rangle\cos\eta + \left\langle\frac{\tilde{s}}{h^2}\sin\eta\right\rangle\sin\eta\right)$$

where $\langle\cdot\rangle = (2\pi)^{-1}\int_0^{2\pi}\cdot\,\mathrm{d}\eta$ is the average over $\eta \in [0, 2\pi]$.

Appendix C: Linear stability of a circle in a shear-thinning fluid

Here we provide detail on the linear stability analysis of a contracting circle in a power-law fluid discussed in section V C. Assume a power law fluid ($n < 1$ shear thinning, $n > 1$ shear thickening), so that

$$\boldsymbol{\sigma} = -p\boldsymbol{I} + \mathcal{A}|D|^{n-1}\boldsymbol{D},$$

29

where $\boldsymbol{\sigma}$ is the stress and $\boldsymbol{D}$ is the strain rate tensor. We scale stresses by $[\sigma] = p^\infty$ and time by $[t]^n = \mathcal{A}/(np^\infty)$, which turns out to be the time scale of the contraction rate of the leading order circle. In polar coordinates, the strain rate is

$$\boldsymbol{D} = \begin{bmatrix} u_r & \frac{1}{2}(v_r + \frac{1}{r}u_\theta - \frac{1}{r}v) \\ \frac{1}{2}(v_r + \frac{1}{r}u_\theta - \frac{1}{r}v) & \frac{1}{r}u + \frac{1}{r}v_\theta \end{bmatrix}$$

where u and v are the radial and azimuthal velocity components, respectively. Note $\frac{1}{r}u + \frac{1}{r}v_\theta = -u_r$ from conservation of mass $\nabla \cdot \boldsymbol{u} = 0$, so $\boldsymbol{D}$ is trace-free. The effective strain rate is $|D| = \sqrt{D_{rr}^2 + D_{r\theta}^2}$. Expanding near a circle: $u \sim u_0(r) + \epsilon\tilde{u}(r,\theta)$, $v \sim \epsilon\tilde{v}(r,\theta)$, etc, we find $|D| \sim u_{0r} + \epsilon\tilde{u}_r$, thus the leading order and correction terms for $\boldsymbol{\sigma}$ are

$$\boldsymbol{\sigma}_0 = \begin{bmatrix} -p_0 + nu_{0r}^n & 0 \\ 0 & -p_0 - nu_{0r}^n \end{bmatrix}$$

$$\tilde{\boldsymbol{\sigma}} = \begin{bmatrix} -\tilde{p} + n^2 u_{0r}^{n-1}\tilde{u}_r & \frac{1}{2}nu_{0r}^{n-1}(\tilde{v}_r + \frac{1}{r}\tilde{u}_\theta - \frac{1}{r}\tilde{v}), \\ \frac{1}{2}nu_{0r}^{n-1}(\tilde{v}_r + \frac{1}{r}\tilde{u}_\theta - \frac{1}{r}\tilde{v}) & -\tilde{p} - n^2 u_{0r}^{n-1}\tilde{u}_r. \end{bmatrix}$$

The governing equation is $\nabla \cdot \boldsymbol{\sigma} = \boldsymbol{0}$. The leading order problem is thus

$$\nabla \cdot \boldsymbol{\sigma}_0 = \begin{bmatrix} \partial_r[-p_0 + nu_{0r}^n] + \frac{2}{r}nu_{0r}^n \\ 0 \end{bmatrix} = \boldsymbol{0}.$$

Conservation of mass implies $u_0 = -B/r$, from which the above and the dimensionless far field condition $p \to 1$ gives

$$p_0 = 1 + \frac{(n-1)B^n}{r^{2n}},$$

where B is still to be determined from the stress boundary condition (see below). The governing equation for the correction terms is

$$\nabla \cdot \tilde{\boldsymbol{\sigma}} = \begin{bmatrix} \partial_r\left[-\tilde{p} + n^2 u_{0r}^{n-1}\tilde{u}_r\right] + \frac{1}{r}\partial_\theta\left[\frac{1}{2}nu_{0r}^{n-1}(\tilde{v}_r + \frac{1}{r}\tilde{u}_\theta - \frac{1}{r}v)\right] + \frac{2}{r}n^2 u_{0r}^{n-1}\tilde{u}_r \\ \partial_r\left[nu_{0r}^{n-1}(\tilde{v}_r + \frac{1}{r}\tilde{u}_\theta - \frac{1}{r}v)\right] + \frac{1}{r}\partial_\theta\left[-\tilde{p} + n^2 u_{0r}^{n-1}\tilde{u}_r\right] + \frac{1}{r}\left(nu_{0r}^{n-1}(\tilde{v}_r + \frac{1}{r}\tilde{u}_\theta - \frac{1}{r}v)\right) \end{bmatrix}$$

$$= \boldsymbol{0}. \tag{C1}$$

While the linear perturbation problem can be solved in closed form, the expressions are complicated enough that we used a Computer Algebra System (Maple) to handle the algebraic manipulation. Consider a mode k perturbation to the circle, that is $s = s_0(t) +$

$\epsilon\tilde{s}(\theta, t)$, where $\tilde{s} = \gamma_k(t)\cos k\theta$. Given the velocity and pressure corrections $\tilde{u}$, $\tilde{v}$ and $\tilde{p}$ must vanish in the far field, they take the form

$$\tilde{u} = (U_1 r^{a_1} + U_2 r^{a_2})\cos k\theta,$$

$$\tilde{v} = (V_1 r^{a_1} + V_2 r^{a_2})\sin k\theta,$$

$$\tilde{p} = (P_1 r^{b_1} + P_2 r^{b_2})\cos k\theta,$$

where $a_j, b_j < 0$. From conservation of mass, $V_j = -(1 + a_j)U_j/k$, and from the governing equation (C1) we find $b_j = a_j + 1 - 2n$ and obtain equations for P_j and a_j. Upon solving,

$$P_j = \frac{1}{2} n B^{n-1} \left(\frac{2a_j{}^2 n - 4a_j n^2 - a_j{}^2 + 6na_j - k^2 + 1}{a_j + 1 - 2n} \right) U_j,$$

and there are four potential solutions for a_j:

$$a_j = (n - 1) \pm \sqrt{2k^2 n - k^2 + n^2 + 2 \pm 2\sqrt{d}}, \tag{C2}$$

$$d = n(n - 1)k^4 - ((n - 1)^2 + n)k^2 + (n - 1)^2.$$

Only two a_j's have negative real part and these may be complex conjugate pairs when $n < 1$ (see figure 9a). We specify a_1 to be the $(-, +)$ case, and a_2 to be the $(-, -)$ case of (C2).

On the free boundary, the stress boundary condition is $\boldsymbol{\sigma} \cdot \boldsymbol{n} = \boldsymbol{0}$. The unit normal to order ϵ is

$$\boldsymbol{n} \sim \begin{bmatrix} 1 \\ 0 \end{bmatrix} + \epsilon \begin{bmatrix} 0 \\ \tilde{s}_\theta/s_0 \end{bmatrix}.$$

The leading order and correction boundary conditions are then

$$\boldsymbol{\sigma}_0 \cdot \boldsymbol{n}_0 = \boldsymbol{0}, \qquad \tilde{\boldsymbol{\sigma}} \cdot \boldsymbol{n}_0 + \tilde{s}\boldsymbol{\sigma}_{0r} \cdot \boldsymbol{n}_0 + \boldsymbol{\sigma}_0 \cdot \tilde{\boldsymbol{n}} = \boldsymbol{0}, \qquad r = s_0.$$

From the leading order stress condition we find $B = s_0^2$. The correction terms determine U_1 and U_2. Finally, the two terms in the expansion of kinematic condition are $\dot{s}_0 = u_0$ and $\tilde{s}_t = \tilde{u} + u_{0r}\tilde{s}$, from which we determine the evolution of s_0 and γ_k:

$$\dot{s}_0 = -s_0, \qquad \dot{\gamma}_k = C_k \gamma_k, \tag{C3}$$

where C_k is given by the rational function

$$C_k = \frac{B}{s_0^2} + \frac{U_1}{\gamma_k} s_0^{a_1} + \frac{U_2}{\gamma_k} s_0^{a_2} = \frac{H_2(k)n^2 + H_1(k)n + H_0(k)}{J_2(k)n^2 + J_1(k)n + J_0(k)}, \tag{C4}$$

31

with the coefficients

$$H_2 = 24k^2 + 8 + 16a_2 + 16a_1 + 8a_1a_2,$$

$$H_1 = (-8a_2 - 8a_1 - 12) k^2 - 4 - 16a_1 - 16a_2 - 8a_2^2 - 20a_1a_2 - 4a_1^2a_2 - 8a_1^2 - 4a_2^2a_1,$$

$$H_0 = -3k^4 + \left(a_2^2 + 2 + 4a_1a_2 + 4a_2 + 4a_1 + a_1^2\right) k^2,$$
$$+ 1 + 4a_2 + 8a_1a_2 + 4a_2^2a_1 + 4a_1 + 3a_1^2 + 4a_1^2a_2 + 3a_2^2 + a_1^2a_2^2,$$

$$J_2 = -8k^2 + 8a_1a_2 + 8,$$

$$J_1 = 4k^2 - 4a_1^2a_2 - 4a_2^2a_1 - 4a_1a_2 - 4,$$

$$J_0 = k^4 + \left(a_1^2 + a_2^2 - 2\right) k^2 + a1^2a_2^2 - a_2^2 - a_1^2 + 1.$$

Returning to dimensional values gives (56).

REFERENCES

[1] J. S. Walder. Röthlisberger channel theory: its origins and consequences. *J. Glaciol.*, 56(200):1079–1086, 2010.

[2] J. Glen. Experiments on the deformation of ice. *J. Glaciol*, 2:111–114, 1952.

[3] H. Röthlisberger. Water pressure in intra- and subglacial channels. *J. Glaciol.*, 11:177–204, 1972.

[4] C. Schoof and I. J. Hewitt. Ice-sheet dynamics. *Ann. Rev. Fluid. Mech.*, 45:217–239, 2013.

[5] J. F. Nye. The flow law of ice from measurements in glacier tunnels, laboratory experiments and the Jungfraufirn borehole experiment. *Proc. R. Soc. Lond. A*, 1953.

[6] C. Schoof. Ice-sheet acceleration driven by melt supply variability. *Nature*, 468:803–806, 2010.

[7] S. Pimentel and G. E. Flowers. A numerical study of hydrologically driven glacier dynamics and subglacial flooding. *Proc. R. Lond. Soc. A*, 467:537–558, 2011.

[8] R. LeB. Hooke, T. Laumann, and J. Kohler. Subglacial water pressures and the shape of subglacial conduits. *J. Glaciol.*, 36(122):67–71, 1990.

[9] F. S. L. Ng. *Mathematical Modelling of Subglacial Drainage and Erosion*. PhD thesis, St. Catherine's College, Oxford University, 1998.

[10] P. M. Cutler. Modelling the evolution of subglacial tunnels due to varying water input. *J. Glaciol*, 44:485–497, 1998.

[11] A. H. Jarosch and M. T. Gudmundsson. A numerical model for meltwater channel evolution in glaciers. *The Cryosphere*, 6:493–503, 2012.

[12] S. Howison. Bibliography of free and moving boundary problems in Hele–Shaw and Stokes flow, August 1998. http://people.maths.ox.ac.uk/howison/Hele-Shaw/.

[13] S. Tanveer and G. L. Vasconcelos. Bubble breakup in two-dimensional Stokes flow. *Phys. Rev. Lett.*, 73(21):2845–2848, 1994.

[14] S. Tanveer and G. L. Vasconcelos. Time-evolving bubbles in two-dimensional Stokes flow. *J. Fluid. Mech.*, 301:325–344, 1995.

[15] D. Crowdy and M. Siegel. Exact solutions for the evolution of a bubble in Stokes flow: a Cauchy transform approach. *SIAM J. Appl. Math.*, 65(3):941–963, 2005.

[16] S. D. Howison, A. A. Lacey, and J. R. Ockendon. Hele–Shaw free-boundary problems with suction. *Q. J. Mech. Appl. Math.*, 41:183–193, 1988.

[17] V. M. Entov, P. L. Etingov, and D. Ya. Kleinbock. On nonlinear interface dynamics in Hele–Shaw flows. *Eur. J. Appl. Math.*, 6(5):399–420, 1995.

[18] M. J. Shelley, F. R. Tian, and K. Wlodarski. Hele–Shaw flow and pattern formation in a time-dependent gap. *Nonlinearity*, 10(6):1471–1495, 1997.

[19] D. G. Crowdy. Exact solutions to the unsteady two-phase Hele–Shaw problem. *Q. J. Mech. Appl. Math.*, 59:475–485, 2006.

[20] S. Kida. Motion of an elliptic vortex in a uniform shear flow. *J. Phys. Soc. Jpn*, 50:3517–3520, 1981.

[21] B. A. Bilby and M. L. Kolbuszewski. The finite deformation of an inhomogeneity in two-dimensional slow viscous incompressible flow. *Proc. R. Soc. Lond. A*, 355:335–353, 1977.

[22] S. Betelú, R. Gratton, and J. Diez. Observation of cusps during the levelling of free surfaces in viscous flows. *J. Fluid Mech.*, 377:137–149, 1998.

[23] C. Pozrikidis. *Boundary integral and singularity methods for linearized viscous flow.* Cambridge University Press, Cambridge, 1992.

[24] C. Pozrikidis. Expansion of a compressible gas bubble in Stokes flow. *J. Fluid Mech.*, 442:171–189, 2001.

[25] C. Pozrikidis. Computation of the pressure inside bubbles and pores in Stokes flow. *J. Fluid Mech.*, 474:319–337, 2003.

[26] H. Ockendon and J. R. Ockendon. *Viscous flow.* Cambridge University Press, Cambridge,

1995.

[27]J. F. Nye. Water flow in glaciers: Jökulhaups, tunnels and veins. *J. Glaciol.*, 17(76):181–207, 1976.

[28]J. D. Gulley, D. I. Benn, E. Screaton, and J. Martin. Mechanisms of englacial conduit formation and their implications for subglacial recharge. *Quaternary Sci. Rev.*, 28:1984–1999, 2009.

[29]D. G. Crowdy. On a class of geometry-driven free boundary problems. *SIAM J. Appl. Math.*, 62:945–954, 2002.